Long-term observations of aerosol optical depth and their relation to in-situ aerosol properties in the Svalbard region (LOAD-RIS)

Georg Hansen[1], Natalia Kouremeti[2], Stefania Gilardoni[3], Kerstin Stebel[1], Nikolaos Evangeliou[1], Christoph Ritter[4], Tymon Zielinski[5], Sara Herrero[6], Stelios Kazadzis[2], David Mateos[6], Mauro Mazzola[3], Paulina Pakszys[5], Konstantinos Eleftheriadis[7]

1 NILU – Norwegian Institute for Air Research, Kjeller, Norway
2 Physikalisch-Meteorologisches Observatorium Davos, World Radiation Center, Davos, Switzerland
3 Institute of Polar Sciences, National Research Council of Italy, Bologna, Italy
4 Alfred Wegener Institute, Helmholtz Centre for Polar and Marine Research, Bremerhaven, Germany
5 Institute of Oceanology of the Polish Academy of Sciences, Sopot, Poland
6 University of Valladolid, Facultad de Ciencias, Valladolid, Spain
7 Environmental Radioactivity Laboratory, NCSR 'Demokritos', Athens, Greece

Corresponding author: Georg Hansen, ghh@nilu.no, georghh@msn.com

Keywords: Aerosols, Arctic haze, biomass burning, black carbon, optical thickness

DOI: https://doi.org/10.5281/zenodo.7376140

1. Introduction

Measurements of aerosol optical depth (AOD) at different wavelengths and the resulting Ångström exponent (AE) by means of sun photometers provide information about the total extinction and, except multimodal aerosols, the size of aerosols in the atmospheric column. This is of great importance for investigations of long-range pollution transport, mostly occurring in the free troposphere. A comprehensive overview of AOD and supplementary in-situ measurements of aerosols both in the Arctic and in Antarctica was given by Tomasi et al. (2015), while an in-depth study of AOD and black carbon (BC) at the three Arctic core sites (Ny-Ålesund, Point Barrow and Alert) in the period 2001–2011 was published by Stone et al. (2014). Recently, Xian et al. (2022 a, b) presented an analysis of (pan-) Arctic spring and summertime AOD trends and extreme events in 2003–2019.

AOD measurements in Svalbard started in 2002 and have continued until today. In other words, a considerable part of the measurements – including the more recent development of increasing summer aerosol load in the Arctic due to biomass burning – is not covered by the above-mentioned publications.

Despite extensive collaboration between groups who have developed the instruments and post-processing algorithms in use, there are different routines both regarding data quality control and cloud flagging, and regarding data aggregation routines (e.g. Kazadzis et al. 2018, Giles et al. 2019). Usually, these challenges are addressed in dedicated inter-comparison campaigns at suitable sites with stable observation conditions, e.g. Izaña Observatory, Tenerife, Spain, for two of the instrument types involved in this project (Cuevas et al. 2019). However, at high-latitude locations, inter-comparison results may differ from those at lower latitudes (Mazzola et al. 2012). Comparing three types of instruments and their respective evaluation routines at one high-latitude location thus offers a valuable contribution to data harmonisation efforts. The value of such an exercise can be further enhanced by also including in-situ measurements of aerosol extinction, absorption and scattering as well as black carbon observations.

In this report, we give an overview over columnar aerosol observations from two sites in Svalbard (Ny-Ålesund, Hornsund) in the time period 2002–2021, links to selected in-situ observations at Gruvebadet Atmosphere Laboratory ('Gruvebadet') and Zeppelin Observatory ('Zeppelin') in Ny-Ålesund, and satellite observations combined with FLEXPART model simulations complementing the two observation methods. The two sites are both located on the western coast of the main island of Spitsbergen, few kilometres into a fjord, but about 200 km apart in N-S direction and, according to a previous study, similar, but not 'identical', in terms of AOD characteristics (Pacszys and Zielinski 2017). However, while at the northern site of Ny-Ålesund sea-ice has been practically absent year-round for more than a decade, sea-ice conditions are still quite variable at Hornsund, due to the strong coastal current there.

2. Data analysis and overview

In the framework of the ReHearsol and the LOAD-RIS projects, AOD and AE datasets were collected from several on- and offshore instruments, AOD usually on 4 wavelengths and AE derived from these. The data sources are listed in Table 1.

Besides AOD and AE measurements, (in-situ) aerosol extinction, absorption and scattering coefficients collected at Gruvebadet (78.918°N, 11.895°E, 30 m a.s.l.) since 2011 and BC extinction coefficients mostly collected at Zeppelin since the 1990s have been included in the data analysis. These are available through the NILU EBAS[1] and the IADC[2] databases.

1 https://ebas.nilu.no/
2 https://iadc.cnr.it/cnr/

Table 1: Sources/instruments of AOD and AE measurements collected in the framework of the ReHearsol/LOAD-RIS projects.

Location	Photometer	Type	Measurement period	Comments
Sverdrup, Ny-Ålesund*	PFR	sun	April 2002–September 2021	1-min. resolution, quality-assured, temperature-stabilised sensor; https://doi.org/10.5281/zenodo.7191072
AWIPEV, Ny-Ålesund**	SP1A	sun	March 2003–October 2020	1-min. resolution, 5 wavelengths out of up to 13 selected
Polish Polar Station, Hornsund***	CIMEL	sun	April 2005–October 2021	2021: level 1.5 quality
AWIPEV, Ny-Ålesund	CIMEL	sun	2017–2021	2021: level 1.5 quality
Zeppelin Observatory, Ny-Ålesund****	SP1A	sun	2015, 2016, 2017, 2019, 2020	10 wavelengths, 4 wavelength AE
AWIPEV, Ny-Ålesund	CIMEL	lunar	2017–2019	
Sverdrup, Ny-Ålesund	PFR	lunar	2018–2020	
on board *R/V Oceania*	Microtops	sun	2007, 2009–2020	geographical area: 72–85°N, 0–50°E
on board *R/V Polarstern*	Microtops	sun	2009, 2012, 2015, 2017, 2020	geographical area: 72–85°N, 0–50°E

*78.923°N, 11.929°E, 5 m a.s.l.
**78.923°N, 11.923°E, 5 m a.s.l.
***77.002°N, 15.540°E, 5 m a.s.l.
****78.907°N, 11.889°E, 475 m a.s.l.

2.1. Inter-comparison of long-term AOD observations in Svalbard

The comparison of the AOD/AE datasets was performed with the primary goal to identify the level of agreement in the collocated instruments and establish an uncertainty level above which AOD spatial differences in the Svalbard area can be considered significant using different instruments, calibration and processing protocols. According to WMO two instruments are equivalent when more than 95% of the compared data show AOD differences within 0.005 ± 0.010/airmass (WMO 2016). This strict limit is difficult to reach at polar monitoring stations due to challenging observation conditions (low temperatures and resulting sensor stability issues, icing) and limited staff.

2.1.1. Comparison of Ny-Ålesund data sets

In Ny-Ålesund, two sun photometers have been run quasi-continuously for 20 years (and more): the SP1A by Alfred Wegener Institute at AWIPEV (since the late 1990s) and the sun PFR at Sverdrup close to AWIPEV (since 2002). In recent years AWI decided to replace the SP1A with a CIMEL instrument; this has been in operation since 2017 and will take over as the only instrument at AWIPEV after a transition period with SP1A and CIMEL running in parallel. In the framework of the ReHearsol project the whole time series of PFR, SP1A and CIMEL measurements has been inter-compared; this has not been done at such a scale at a polar station so far. The overall comparison results are summarised in Table 2, while details about this exercise are given in Appendix 1. For Ny-Ålesund we consider 66% of the AOD differences between different instruments being within the WMO limits as a statistically significant and satisfactory agreement given the conditions of the station.

In Figure 1 the level of agreement of the compared instruments is presented as median AOD differences at four wavelengths over each year along with the 5th and 95th percentiles (error bars). The filled symbols indicate that more than 66% (small) and 95% (large) of the compared values are within the WMO limit. It is evident that the level of agreement between SP1A and PFR has significantly improved since 2009. For the CIMEL-AWIPEV the highest level of agreement is observed in 2017

Table 2: Summary of long-term AOD differences between PFR, SP1A and CIMEL sun photometer at Ny-Ålesund. For wavelength pairs marked with * PFR values were interpolated to match CIMEL wavelengths, using the PFR AE.

	Wavelength/nm	AOD difference			% within WMO limits	Correlation Coefficient
		Median	5th percentile	95th percentile		
PFR-SP1A	368/368	0.002	-0.034	0.023	51.4	0.93
	412/412	0.007	-0.029	0.031	40.0	0.91
	500/500	0.006	-0.017	0.026	48.3	0.90
	862/862	0.001	-0.017	0.017	68.7	0.69
PFR-CIMEL	367/380*	0.013	0.004	0.027	26.5	0.99
	412/440*	0.013	0.005	0.028	19.2	0.98
	500/500	0.007	0.002	0.017	63.9	0.98
	862/870	0.002	-0.002	0.010	92.5	0.94

and 2018 (AERONET level-2 product) especially for the common wavelengths 500 nm and 870 nm, almost reaching or exceeding the WMO traceability criterium (91% to 99%). The level of agreement of the instruments poses difficulties in merging the datasets, but it is possible to fill gaps due to technical failures and secure continuous AOD measurements at Ny-Ålesund, at least in the near-infrared wavelength (870 nm). The overall comparison results are summarised in Table 2.

2.1.2. Comparison of SP1A observations at AWIPEV and Zeppelin Observatory

Since 2015, sun photometer measurements by means of an SP1A instrument have also been carried out at Zeppelin. Here we present a comparison for the year 2017, in which 25 480 isochronal (time difference < 10 minutes) one-minute measurements are available during the whole sunlit season.

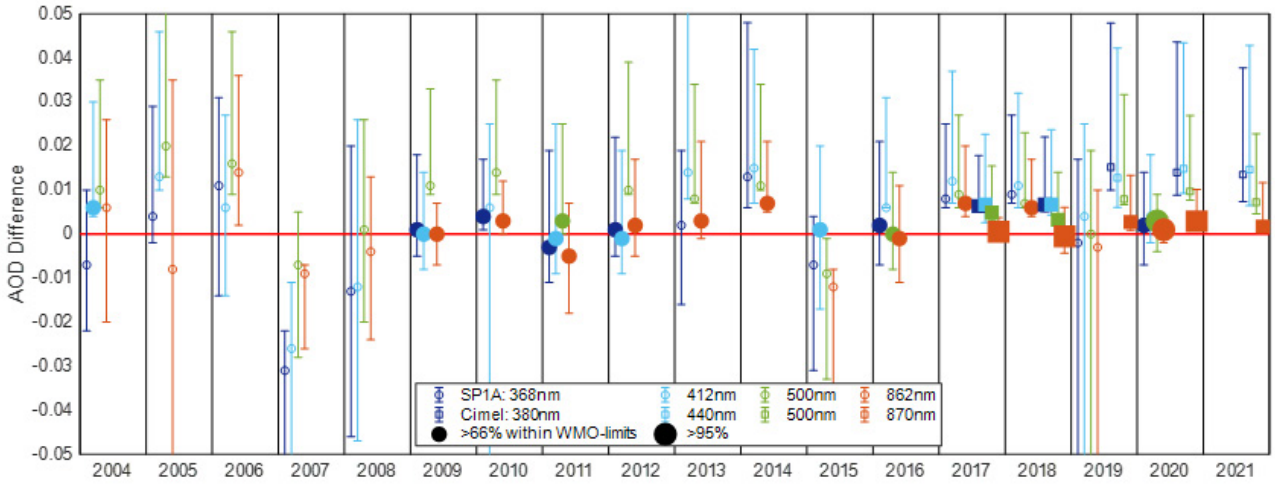

Figure 1: Yearly median AOD difference at four wavelengths for the SP1A (open circles) and CIMEL (open squares). The error bars represent the 5th and 95th percentile of the differences observed with in the year. The small and big filled circles and squares indicate datasets with agreement within the WMO uncertainty limit to better than 66% and 95%, respectively. Red line: zero difference level.

The AOD at 500 nm measured at AWIPEV ('Ny-Ålesund', in blue) and the difference between these and the corresponding measurements from Zeppelin (in red) are shown in Figure 2. Obviously, the AOD absolute differences between both sites are small. At 500 nm the median AOD at Zeppelin is 0.0033 (7.55%) lower than at AWIPEV. Only in 12.1% of all cases is the AOD difference larger than 0.01. The correlation between the two AOD at 500 nm data series over time is r = 0.9596, and at 368 nm it is even larger (0.9709). Moreover, we found that the small difference in AOD does not depend on the AOD itself. This means that observations at Zeppelin do not simply miss a constant fraction of aerosol. Instead, based on this work, one can expect that the aerosol in-situ samplers at Zeppelin and at Gruvebadet, averaged over a season, should measure almost the same aerosol in accumulation and coarse mode.

On the other hand, the Ångström exponent values (not shown here) reveal slight differences: Whenever the Ångström exponent (at Zeppelin) is larger than 1.5 it is even higher at, indicating that Zeppelin is missing some of the newly formed particles in the Aitken mode from the ocean in summer.

2.1.3. Comparison of Hornsund CIMEL data with Ny-Ålesund CIMEL data

A comprehensive analysis of aerosol measurements in the Svalbard region in the years 2000–2015 was made in the PhD thesis of Dr. Paulina Pakszys (2018); the comparison between Hornsund and Ny-Ålesund in the same period is discussed in Pakszys and Zielinski (2017). Both studies concluded with a generally high correlation between AOD observations at the two sites, but with a bias towards slightly higher mean values and larger variability at Hornsund. These analyses were based on different instruments at the two sites. From 2017, data from the same instrument type with identical calibration and analysis procedures (AERONET) became available, allowing a direct and simultaneous comparison of AOD at the two AERONET sites.

A total of 180 data pairs were obtained in the period 2017–2019. To increase this number we decided to use level 1.5 data (upgraded to level 2 data shortly before the end of the project period); this yielded 849 data pairs instead. Results from this enhanced data set are shown for two wavelengths in Figure 3; level 2.0 data results agree with this. The statistics of the comparison show Mean Bias Error (MBE) values below 0.009 for all channels and Root Mean Square Error (RMSE) values ranging from 0.02 at 1020 nm to 0.29 at 340 nm. Overall, about half of the differences are within the WMO U95 limits (analysis not shown here) despite the distance between two sites. However, the other half of the data proves that different aerosol conditions are measured frequently at the two sites. Generally, AOD values are slightly larger at Hornsund than at Ny-Ålesund, especially at shorter wavelengths.

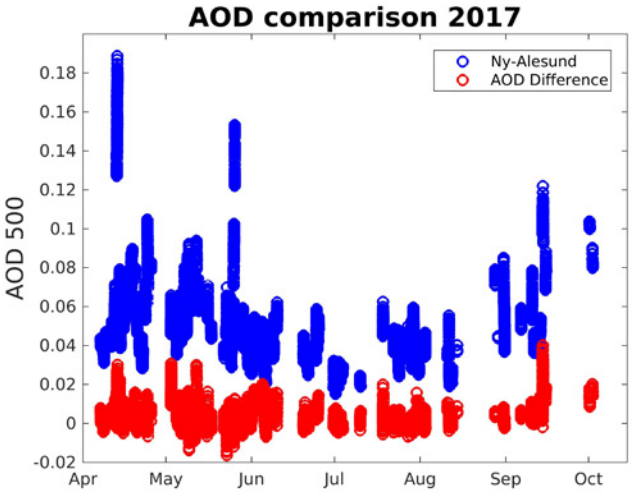

Figure 2: SP1A AOD observations at 500 nm in 2017 at AWIPEV, Ny-Ålesund (blue) and difference AOD (AWIPEV) – AOD (Zeppelin) (red).

2.2. High-AOD episodes

Initially, a threshold value of 0.15 for AOD at 500 nm was chosen to identify high-AOD events. All hourly means >0.1 and >0.15 (for moderate and high AOD events) from all instruments were identified and stored in annual files. Moreover, annual files listing all single measurements of AOD (500 nm) >0.1 and >0.15, respectively, from all instruments were created. Figure 4 shows the percentage of AOD hourly means >0.15 for four instruments included in the analysis (Ny-Ålesund: PFR, SP1A, CIMEL; Hornsund: CIMEL), the left panel from the period March–May and the right panel from the period June–August. The most prominent feature

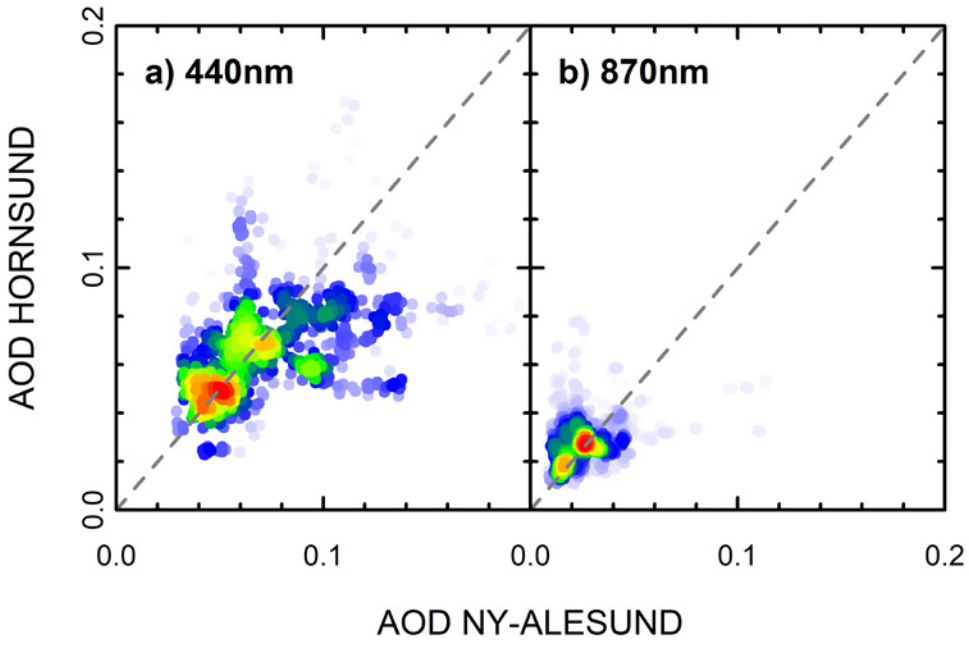

Figure 3: AOD scatterplot between CIMEL measurements in Hornsund and Ny-Ålesund at two wavelengths (440 nm, 870 nm). Colour scale indicates the density concentration from high (red) to low (blue).

is the decrease in number of high-AOD episodes in the March–May period since the early 2000s. In the June–August period there is no clear trend, but a tendency towards more frequent high-AOD episodes since 2014, with 2019 as a case of exceptionally persistent high-AOD conditions both in Ny-Ålesund and in Hornsund. We propose this is related to more frequent summer biomass burning episodes which more easily reach Hornsund (200 km closer to the Eurasian mainland).

Observations of aerosol originating from biomass burning events have been published for selected cases. The most prominent is the spring 2006 event which caused unprecedented levels of pollution in Svalbard (e.g. Stohl et al. 2007). More typical summer episodes originating from boreal forest fires in North America and Siberia in 2015 and 2017, respectively, were analysed and published by Markowicz et al. (2016) and Zielinski et al. (2020).

2.2.1. Comparison of columnar and in-situ aerosol properties at Ny-Ålesund – Arctic haze vs. summer biomass burning events

To better characterise the observed columnar aerosol, the AOD data were compared with aerosol properties derived from in-situ measurements, including aerosol absorption, scattering and extinction coefficients from Gruvebadet, and aerosol absorption coefficients from Zeppelin. Gruvebadet is located at about 1 km from the Ny-Ålesund settlement at 30 m a.s.l., while Zeppelin is sited at the top of the Zeppelin Mountain at 474 m a.s.l., about 2 km from the coast and 1 km from Gruvebadet. Aerosol absorption coefficient time series at Zeppelin and Gruvebadet are described, e.g. in Eleftheriadis et al. (2009) and Stathopoulos et al. (2021), while the chapter 'ABC Svalbard' in SESS report 2019 (Gilardoni et al. 2020) compares the time series at the two sites.

To compare aerosol properties depending on the aerosol load, three aerosol situations have been distinguished using columnar information: low, moderate, and extreme AOD. Following an automatic methodology proposed by Mateos et al. (2020) and based on an AERONET AOD measurement strategy with a quality-control algorithm (Giles et al. 2019), AOD for fine and coarse modes at 500 nm (AOD_F and AOD_C respectively), are analysed for hourly data from Ny-Ålesund. If AOD_F is higher than the 85th percentile of all the time series or AOD_C is higher than the 93rd percentile (we select a higher percentile because of the lower probability that this mode will appear at the current location) an aerosol event is identified. When considering only those events with a total AOD (500 nm) <0.15, a mean value of AOD (500 nm) of 0.1 for them is obtained, which has been selected as threshold for moderate

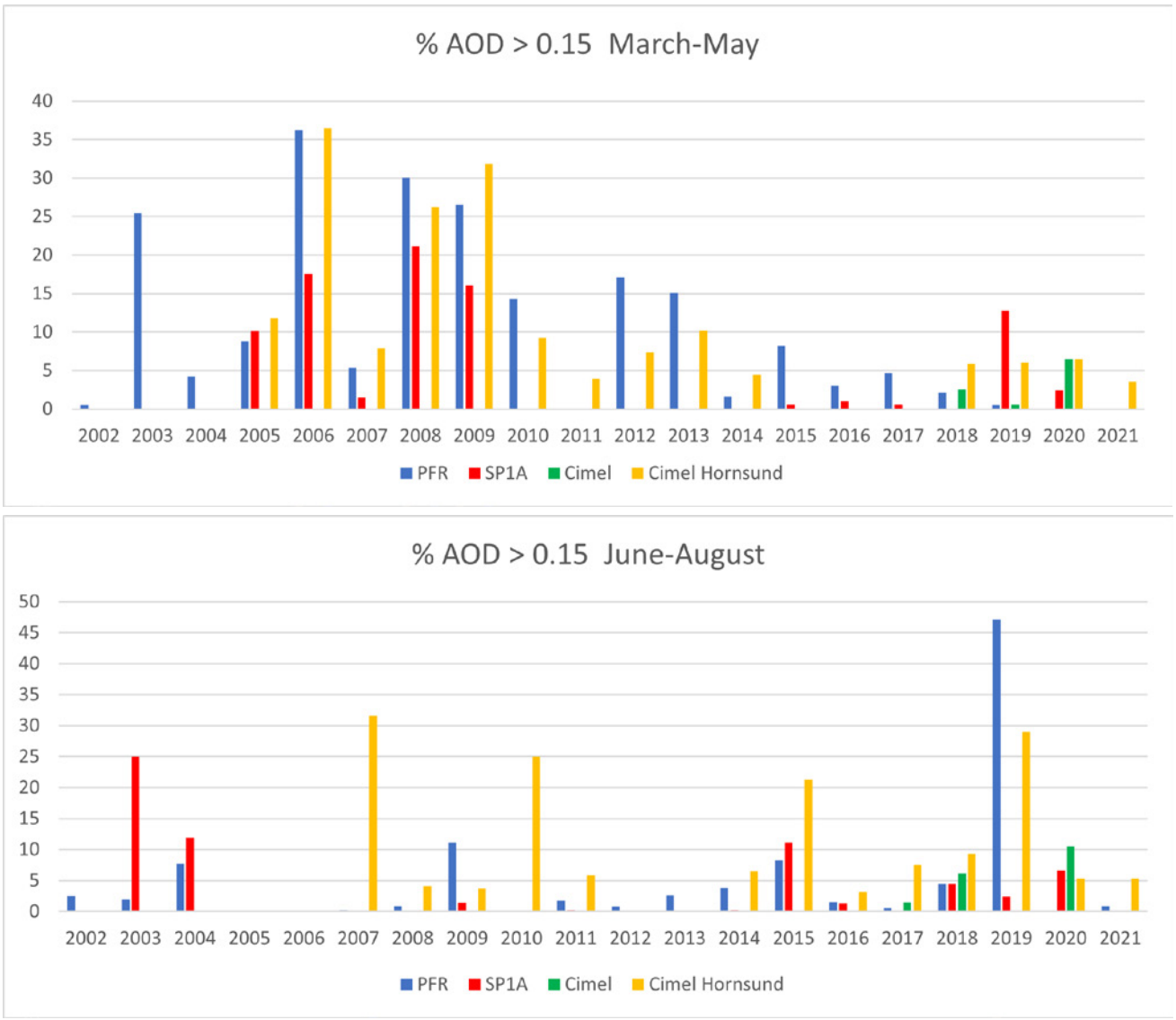

Figure 4: Frequency of high-AOD (>0.15 at 500 nm) episodes in the periods March–May (left panel) and June–August (right panel) for 4 sun photometers (3 in Ny-Ålesund, 1 in Hornsund). The CIMEL in Ny-Ålesund started operations in June 2017.

conditions. Therefore, a columnar low aerosol load is considered if the total AOD (500 nm) is below 0.1. If only those events with total AOD (500 nm) >0.15 are considered, a mean value of 0.24 is obtained, which has been selected as threshold for extreme conditions. Columnar moderate aerosol events correspond to total AOD between 0.1 and 0.24. And finally, columnar extreme aerosol events are those showing an AOD (500 nm) larger than 0.24.

Figure 5 compares the aerosol scattering, absorption, and extinction coefficients at 530 nm measured at the ground sites during periods characterised by low, moderate, and high AOD. The period from 9 July to 28 August 2019 was excluded from the analysis and is addressed separately. In general, higher coefficients are observed for moderate and high AOD episodes, with statistically significant differences compared to low-AOD periods (significance level 0.05). Differences are more pronounced for scattering and extinction coefficients, and during extreme AOD events.

We identified the time periods characterised by high aerosol extinction coefficient at ground level as those days characterised by coefficient values larger than the de-seasonalised average plus three times the standard deviation of the average. The comparison between the occurrences of moderate and high AOD and high extinction coefficient values indicate that a small fraction of aerosol transport episodes to Svalbard are detected at the

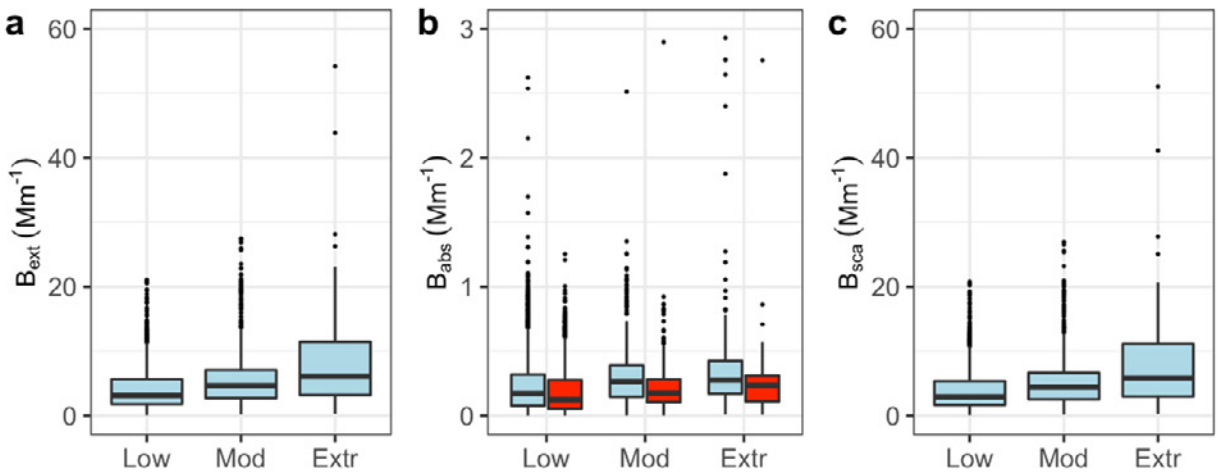

Figure 5: Box-whisker plot of extinction (panel a) absorption (panel b) and scattering (panel c) coefficients at Gruvebadet (in light blue) and Zeppelin (in red) during low, moderate and high AOD episodes. The box identifies the 25th and 75th percentile, the line inside the box corresponds to the median, the vertical lines extend to the minimum and maximum without outliers, while the dots indicate outliers. Gruvebadet and Zeppelin time series overlap partially and a direct comparison of the two sites is not discussed in this context.

ground. Depending on the AOD record, 67–89% of the moderate and high AOD events were not associated with a significant increase of the in-situ aerosol extinction coefficient (Hansen et al. 2022).

PFR AOD measurements in Ny-Ålesund, CIMEL measurements in Hornsund and Microtops measurements on board the research vessel *Oceania* in the Fram Strait revealed significantly elevated AOD values almost continuously from early July to early September 2019 (see Figure 6). For comparison, the 20-year monthly mean AOD values (PFR) are also included in the figure, proving that summer 2019 was exceptional, with July and August monthly means 2 to 3 times higher than long-term means. The general agreement between the three observation sites indicates that this must have been due to large-scale presence of aerosols. High aerosol loading was simultaneously observed by integrated column and in-situ measurements on 7–9 July, 17 July, and 5 August, but many high-AOD observations later in August are not seen in the in-situ data. The only way to clarify this discrepancy is through information about the altitude of the aerosol layer, which can be obtained from ground-based lidar (dependent on clear-sky conditions) and from space-based lidar observations.

2.2.2. Satellite observations of high-AOD episodes over Svalbard: a case study from July/August 2019

Satellite data can be of great value both to complement total column data in periods of cloudy ground conditions (caveat: AOD data usually are only derived for cloud-, ice- and snow-free pixels) and to identify the altitude distribution of aerosols and thus cast light on when AOD and in-situ measurements can be combined. Vertical profile information on aerosol extinction and polarisation can be obtained from the Cloud-Aerosol Lidar with Orthogonal Polarisation (CALIOP) on board the Cloud-Aerosol Lidar and Infrared Pathfinder Satellite Observations (CALIPSO) platform (Winker et al. 2009). Furthermore, the V4 level 2 cloud–aerosol discrimination (CAD) algorithm distinguishes between tropospheric and stratospheric aerosol subtypes (Kim et al. 2018). The data were downloaded from the ICARE Data and Services Center[3].

In Figure 7, we show two examples of level 2 data (version 4.20) curtains of the aerosol extinction at 532 nm to evaluate the vertical representation of the aerosols during the 2019 high-AOD episodes. White areas present regions with no signal (clouds inhibiting the observations below), clouds

3 https://www.icare.univ-lille.fr, last access: 08 August 2022

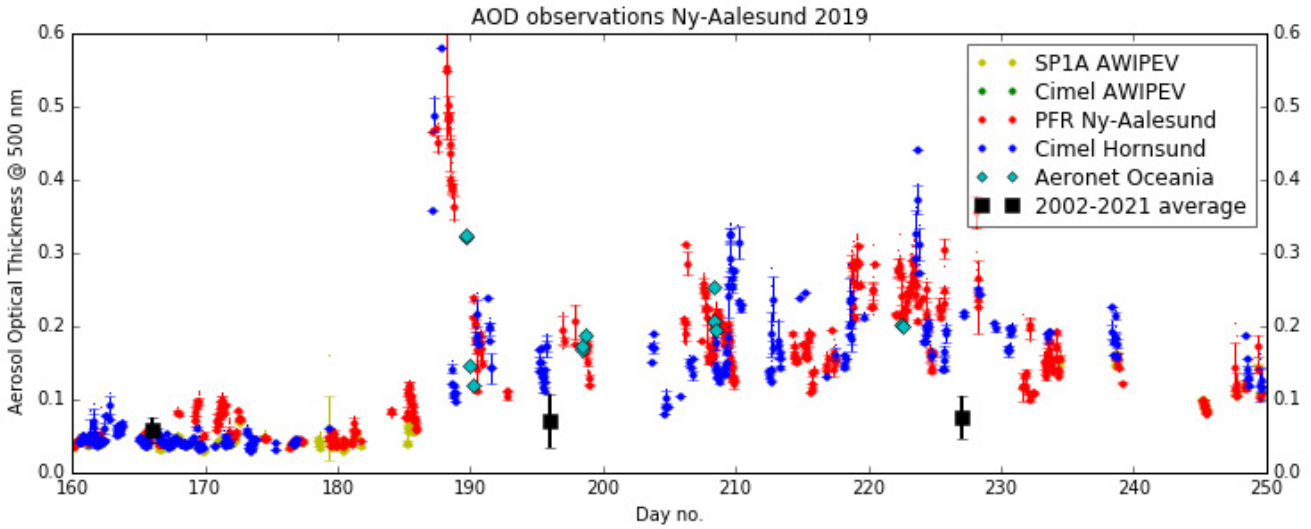

Figure 6: AOD measurements (hourly means with standard deviation of single measurements) performed in and around Svalbard in summer 2019 (9 June–6 September), with data from Ny-Ålesund, Hornsund and *R/V Oceania* (in the Fram Strait). Long-term monthly means of PFR measurements in Ny-Ålesund are shown as black squares with error bars. No CIMEL measurements were made in Ny-Ålesund in this time interval of 2019.

in the respective area or no aerosols. The most prominent case is from 6–7 July, with by far most PFR measurements on 7 July starting at 05:00 with values of around 0.5 (at 500 nm) and continuing until around 18:00 with AOD dropping to 0.36. On that occasion there are few data from Hornsund. On 7 July 03:15 UTC there was a CALIPSO overpass over Svalbard, close to Ny-Ålesund. Low-level clouds were obstructing the scenes between Ny-Ålesund and Hornsund, around 13°E and the view below 3 km altitude at Ny-Ålesund. The tropospheric aerosol layer reaching up to about 4 km altitude above Svalbard was classified as elevated smoke. A second, extended, period of high AOD values at Ny-Ålesund occurred from 6 (from 17:00) to 11 August (until 16:00), with AOD hourly means ranging from 0.2 to 0.31. There are few data from Hornsund at the beginning and end of the period which fit into the Ny-Ålesund measurements. Here, we show an example of a CALIOP curtain above Svalbard from the morning of 6 August, 09:05 UTC. Also on this occasion cloud cover around 5 km altitude obstructs some of the lower tropospheric aerosol observations over mid-/west Svalbard. The thick aerosol layer at 4–5 km altitude west of Svalbard is classified as elevated smoke, the three layers between Ny-Ålesund and Hornsund at about 6–7 km altitude are labelled as dust, polluted dust, and elevated smoke.

As an additional complication, a stratospheric sulphate aerosol layer occurred in summer 2019. This aerosol which could be observed from mid-July onward, was caused by the Raikoke volcano on the Kuril Islands in the western Pacific Ocean, which had a series of eruptions on 21–22 June 2019. The layer contributed an estimated AOD of up to 0.03 at 500 nm from mid-July to the end of August, i.e. exactly in the period with elevated AOD values in Svalbard, but it cannot alone explain the elevated AOD summer values seen in Figure 6. The event is discussed in detail in a recent publication by Kloss et al. (2021). Not considered here is the potential self-lifting of the large forest fires in Siberia, which could have caused an ascent of the smoke layer into the lower stratosphere, potentially leading to a misclassification of the CALIOP aerosol typing (see Ansmann et al. 2021).

2.2.3. Aerosol back-trajectory studies: A case study of the summer 2019 event

To investigate the possible origin of the aerosols on the two occasions presented in the previous section, the Lagrangian particle dispersion model FLEXPART (FLEXible PARTicle dispersion model) version 10.4 was used (Pisso et al. 2019). The model was driven by 3-hourly operational meteorological fields from the European Centre for Medium-Range Weather Forecasts (ECMWF) with 137 vertical

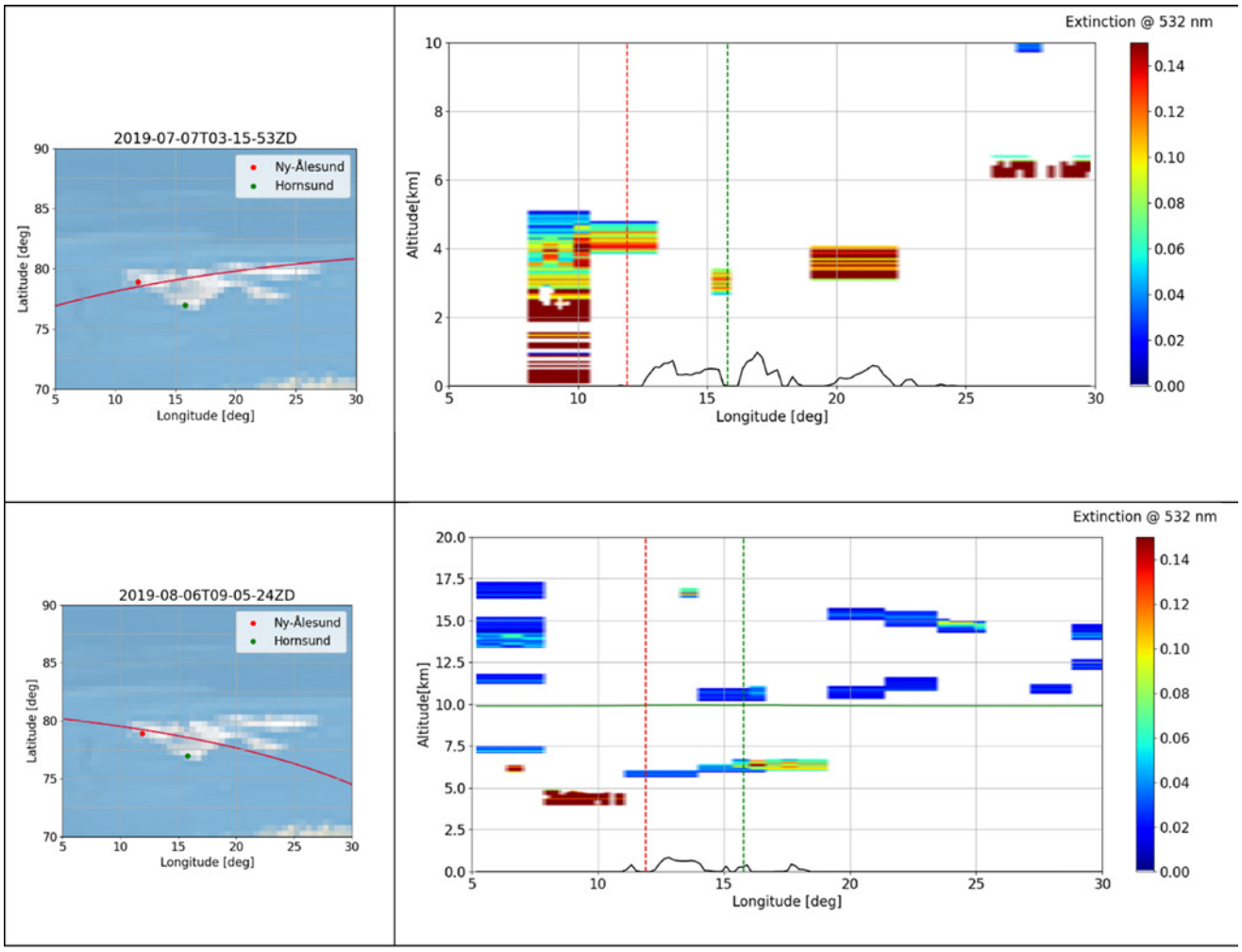

Figure 7: Aerosol extinction at 532 nm [units: km^{-1}] during two CALIOP overpasses (left panels: satellite geo-location): 7 July 2019, 03:15 (upper panel) and 6 August 2019, 09:05 (lower panel). Vertical dashed lines: ground station longitudes (red: Ny-Ålesund, green: Hornsund). Left panels: satellite geolocation maps.

levels and a horizontal resolution of 1°×1°. In FLEXPART, computational particles are released at the altitudes where they were detected by CALIOP and are tracked backward in time in FLEXPART's 'retroplume' mode. Simulations extended over 10 days backward in time, sufficient to include aerosol emissions from biomass burning arriving at the measurement site, given a typical aerosol lifetime of 1 week (Bond et al. 2013). The tracking includes gravitational settling for spherical particles of the size observed. FLEXPART differs from trajectory models due to its ability to simulate dry and wet deposition of gases or aerosols, turbulence, unresolved mesoscale motions, while it includes a deep convection scheme (see Pisso et al. 2019). For our simulations, we assumed that aerosols have a density of 1500 kg/m^3 (similar to black carbon) and follow a logarithmic size distribution with an aerodynamic mean diameter of 0.25 µm and a logarithmic standard deviation of 0.3 (Long et al. 2013).

Figure 8, left panel, shows the result for 7 July, 03:00 UTC, for an assumed aerosol height above Ny-Ålesund of 4–4.5 km. As the plume altitude was not known, the integrated footprint from 1 to 10 km was used. The figure shows a well-defined source region in Central Siberia which coincides very well with the location of extensive forest fires at the end of June and early July. The aerosols moved essentially straight northeastward towards Svalbard. This pattern was geographically very stable throughout 7 July. On 6 August, shown for one time slot in Figure 8, right panel, the situation was very different. On this day, the back-trajectories, now with a release height of 6 to 6.5 km, point towards northern Canada and Alaska, with an extension towards Siberia. In this

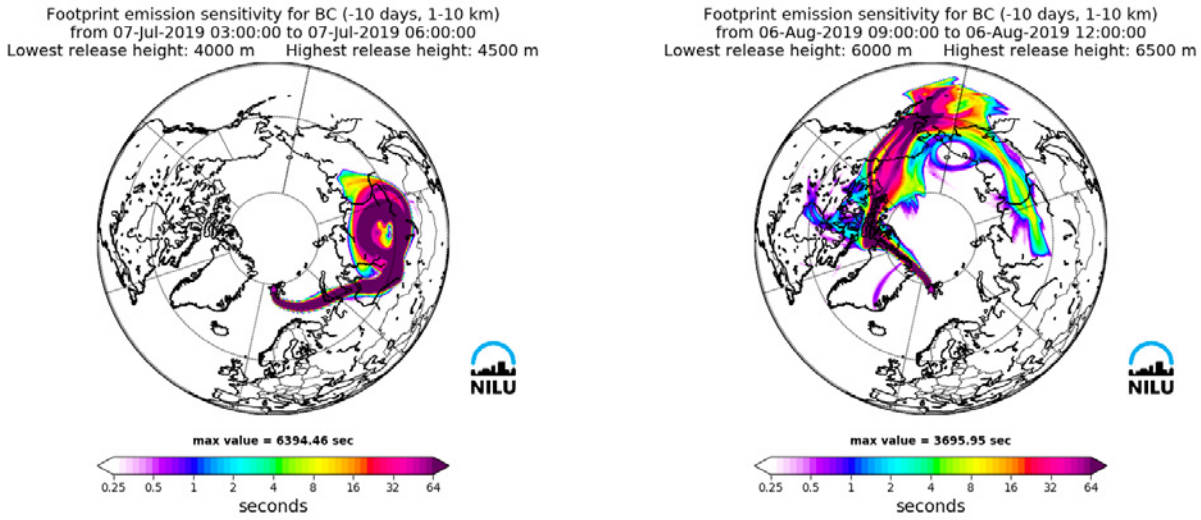

Figure 8: FLEXPART 10-day back-trajectory calculation of aerosols observed on 7 July (left panel) and 6 August (right panel), 2019.

case, the 10-day limitation probably was too short to mark Siberia as the origin of the aerosol; in Alaska, there were few fires in the 10 days prior to 6 August. There are also differences between Ny-Ålesund and Hornsund on this day, with clearly lower AOD values in the morning of 6 August over Hornsund increasing throughout the day. Back-trajectories from Hornsund show source regions over Greenland and the northwestern Atlantic for the morning of 6 August, then shifting to the same pattern as in Ny-Ålesund over the day, at the same time as AOD values reach the same level as in Ny-Ålesund.

These few samples of ground-based, satellite and model data show the potential of combining such data, but also the complexity to be considered. For example, we have not discussed here the possible contribution of the volcano aerosols mentioned above or the impact of deep injection processes of fire aerosols possibly reaching the lower stratosphere. The situation of summer 2019 definitely deserves a much more careful analysis than is possible within the scope of this SESS chapter. Thus, developing adequate tools for such occasions, which probably will occur more frequently in the future, will serve studies using a wide range of observations.

3. Contributions to interdisciplinarity

Aerosols and their effect on the atmosphere are an important aspect of the climate system, influencing both solar irradiation and formation of cloud nuclei with further implications on cloudiness. In the most recent published assessment (AR6) of the IPCC (IPCC 2021) the contribution from aerosols to changes in effective radiative forcing since 1750 remains the one with the largest uncertainty, especially the contribution of aerosol–cloud interactions. In the polar areas this uncertainty is even greater. During winter conditions, aerosol can warm the surface, favouring cloud formation and trapping long-wave radiation. In spring, deposition of light-absorbing aerosol reduces snow and ice albedo, accelerating their melting (e.g. Skiles et al. 2018). Finally, in spring and summer, aerosol contributes to scattering and absorption of incoming short-wave radiation, in addition to altering cloud properties. An improved monitoring of aerosol load will contribute to reducing these uncertainties. A second important field of interdisciplinary research is that of aerosols as a carrier of pollution from lower to high latitudes, i.e. from regions with high pollution load to those with little local and regional pollution (although also this pattern is changing with the increasing number of biomass burning events in the boreal zone).

4. Unanswered questions

Although the different photometers presented in this study do agree quite well in general, noticeable differences have been observed. The dominance of small-scale, micrometeorological phenomena in fjords affects sites like Ny-Ålesund and Hornsund in a complex manner, e.g. through aerosol advection at different altitudes. Potential resulting differences between the various AOD data sets are not yet fully understood, and efforts should continue to clarify these.

The closure between aerosol properties derived by in-situ and remote sensing instruments is still a challenging topic. Thanks to their very high time resolution and their availability at different places in and around Ny-Ålesund, photometer data are helpful to interpret, e.g. filter-based aerosol measurements in terms of uniform conditions or consistency.

The fraction of aerosol, which is principally missed by in-situ measurements due to advection altitudes in the free troposphere or even stratosphere is hard to assess. If the optical properties of aerosol at the ground and the height and stability of the boundary layer were known, the photometers could easily estimate the aerosol fraction aloft.

So far, there are far fewer AOD observations during polar night. This report is based on sun-photometer data. Hence a significant part of the annual cycle (about 5 months of the year) is still severely under-represented.

5. Recommendations for the future

- Sun AOD measurements should continue at both Hornsund and Ny-Ålesund as at present, while a third station in eastern Svalbard connected to a meteorological station should be established;
- An observation capacity on board a mobile platform (UAV, aircraft) with the possibility to perform limited campaigns during periods of elevated AOD measurements should be developed and stationed at Ny-Ålesund or Longyearbyen;
- More emphasis should be put on collecting data during the polar night, possibly through the establishment of a star photometer and further development of lunar AOD observations.
- Efforts to integrate in-situ, columnar, lidar (which have been performed at AWIPEV for many years), and satellite remote-sensing observations and combining them with various modelling tools such as FLEXPART should be intensified and streamlined for near-real-time applications in high-AOD episodes.

6. Data availability

Dataset	Parameter	Period	Location	Metadata access (URL)	Dataset contact
Aggregated AOD/ AE data from the Svalbard region	Aeorosol Optical Depth (4/5 wavelengths), Ångström Exponent	2002-2021	Sverdrup, AWIPEV (both Ny-Ålesund), Polish Polar Station (Hornsund)	https://doi.org/10.21343/1GAJ-4645	Kerstin Stebel (NILU) kst@nilu.no
Gruvebadet Atmosphere Laboratory data	Aerosol absorption coefficient and aerosol scattering coefficient	2010-2020	Gruvebadet	https://metadata.iadc.cnr.it/geonetwork/srv/eng/catalog.search#/metadata/ee3fb49e-c3e2-4572-95b8-1e7ff6361ac5 https://metadata.iadc.cnr.it/geonetwork/srv/eng/catalog.search#/metadata/534d6e9e-8bb5-40d1-8ddd-1092e0373584	Stefania Gilardoni (IPS-CNR) stefania.gilardoni@cnr.it
Zeppelin Observatory data	Aerosol absorption coefficient	2005-2021	Zeppelin Mt	https://ebas-data.nilu.no/Pages/DataSetList.aspx?key=8AFF59A5D-0A845C7833AE6F65D-990D5C	Kostas Eleftheriadis (NCSR Demokritos) eleftheriadis@ipta.demokritos.gr

7. Acknowledgements

This work was supported by the Research Council of Norway, project number 322387, Svalbard Integrated Arctic Earth Observing System – Knowledge Centre, operational phase 2022. We are grateful for the technical support from the Norwegian Polar Institute for the PFR measurements in Ny-Ålesund and in-situ measurements at Zeppelin Observatory. We also gratefully acknowledge the use of imagery provided by services from NASA's Global Imagery Browse Services (GIBS), part of NASA's Earth Observing System Data and Information System (EOSDIS).

8. References

Ansmann A, Ohneiser K, Chudnovsky A, Baars H, Engelmann R (2021) CALIPSO Aerosol-Typing Scheme Misclassified Stratospheric Fire Smoke: Case Study From the 2019 Siberian Wildfire Season. Front Environ Sci 9:769852. https://doi.org/10.3389/fenvs.2021.769852

Bond TC, Doherty SJ, Fahey DW, Forster PM, Berntsen T, DeAngelo BJ et al (2013) Bounding the role of black carbon in the climate system: A scientific assessment. J Geophys Res Atmos 118(11):5380-5552. https://doi.org/10.1002/jgrd.50171

Cuevas E, Romero-Campos PM, Kouremeti N Kazadzis S, Räisänen P, Garcia RD, Barretto A, Guirado-Fuentes C, Ramos R, Toledano C, Almansa F, Grübner J (2019) Aerosol optical depth comparison between GAW-PFR and AERONET-Cimel radiometers from long-term (2005-2015) 1 min synchronous measurements. Atmos Meas Tech 12:4309-4337. https://doi.org/10.5194/amt-12-4309-2019

Eleftheriadis K, Vratolis S, Nyeki S (2009) Aerosol black carbon in the European Arctic: Measurements at Zeppelin station, Ny-Ålesund, Svalbard from 1998–2007. Geophys Res Lett 36(2). https://doi.org/10.1029/2008GL035741

Gilardoni S, Lupi A, Mazzola M, Cappelletti DM, Moroni B, Ferrero L, Markuszewski P, Rozwadowska A, Krecji R, Zieger P, Tunved P, Karlsson L, Vratolis S, Eleftheriadis K, Viola AP (2020) Atmospheric black carbon in Svalbard. In: Van den Heuvel et al. (eds): SESS report 2019, Svalbard Integrated Arctic Earth Observing System, Longyearbyen, pp 196–211. https://doi.org/10.5281/zenodo.4707201

Giles DM, Sinyuk A, Sorokin MG, Schafer JS, Smirnov A, Slutsker I, Eck TF, Holben BN, Lewis JR, Campbell JR, Welton EJ, Korkin SV, Lyapustin AI (2019) Advancements in the Aerosol Robotic Network (AERONET) Version 3 database

– automated near-real-time quality control algorithm with improved cloud screening for Sun photometer aerosol optical depth (AOD) measurements. Atmos Meas Tech 12:169-209. https://doi.org/10.5194/amt-12-169-2019

Hansen GH, Zielinski T, Pakszys P, Rittre C, Gilardoni S, Eleftheriadis K, Kouremeti N, Mateos D, Herrero S, Kazadzis S, Mazzola M, Stebel K (2022) Re-evaluation and Homogenization of Aerosol Optical Depth Observations in Svalbard (ReHearsol). RCN Project No: 311250/E40 - ReHearsol Final Report (NILU report 03/2022). Kjeller: NILU

Holben BN, Eck TF, Slutsker I, Tanré D, Buis JP, Setzer A, Vermote E, Reagan JA, Kaufman YJ, Nakajima T, Lavenu F, Jankowski I, Smirnov A (1998) AERONET – A Federated Instrument Network and Data Archive for Aerosol Characterization. Rem Sens Envir 66(1):1-16. https://doi.org/10.1016/S0034-4257(98)00031-5

IPCC (2021) Climate Change 2021: The Physical Science Basis. Contribution of Working Group I to the Sixth Assessment Report of the Intergovernmental Panel on Climate Change. Masson-Delmotte V, Zhai P, Pirani A et al (eds) Cambridge: Cambridge University Press. In Press

Kazadzis S, Kouremeti N, Nyeki S, Gröbner J, Wehrli C (2018) The World Optical Depth Research and Calibration Center (WORCC) quality assurance and quality control of GAW-PFR AOD measurements. Geosci Instrum Method Data Syst 7(1):39-53. https://doi.org/10.5194/gi-7-39-2018

Kim M-H, Omar AH, Tackett JL et al (2018) The CALIPSO version 4 automated aerosol classification and lidar ratio selection algorithm Atmos Meas Tech 11:6107-6135. https://doi.org/10.5194/amt-11-6107-2018

Kloss C, Berthet G, Sellitto P et al (2021) Stratospheric aerosol layer perturbation caused by the 2019 Raikoke and Ulawun eruptions and their radiative forcing. Atmos Chem Phys 21:535-560. https://doi.org/10.5194/acp-21-535-2021

Long CM, Nascarella MA, Valberg PA (2013) Carbon black vs. black carbon and other airborne materials containing elemental carbon: Physical and chemical distinctions. Environ Pollut 181:271-286. https://doi.org/10.1016/j.envpol.2013.06.009

Markowicz KM, Pakszys P, Ritter C et al (2016) Impact of North American intense fires on aerosol optical properties measured over the European Arctic in July 2015. J Geophys Res Atmos 121(24):14487-14512. https://doi.org/10.1002/2016JD025310

Mateos D, Cachorro VE, Velasco-Merino C et al (2020) Comparison of three different methodologies for the identification of high atmospheric turbidity episodes. Atmos Res 237(26):104835. https://doi.org/10.1016/j.atmosres.2019.104835

Mazzola M, Stone RS, Herber A et al (2012) Evaluation of sun photometer capabilities for retrievals of aerosol optical depth at high latitudes: The POLAR-AOD intercomparison campaigns. Atmos Env 52:4-17. https://doi.org/10.1016/j.atmosenv.2011.07.042

Pacszys P, Zielinski T (2017) Aerosol optical properties over Svalbard: a comparison between Ny-Ålesund and Hornsund. Oceanologia 59(4):431-444. https://doi.org/10.1016/j.oceano.2017.05.002 Pisso I, Sollum E, Grythe H (2019) The Lagrangian particle dispersion model FLEXPART version 10.4, Geosci Model Dev 12:4955-4997. https://doi.org/10.5194/gmd-12-4955-2019

Skiles SM, Flanner M, Cook JM, Dumont M, Painter TH (2018) Radiative forcing by light-absorbing particles in snow. Nature Climate Change 8:964-971. https://doi.org/10.1038/s41558-018-0296-5

Stathopoulos VK, Evangeliou N, Stohl A, Vratolis S, Matsoukas C, Eleftheriadis K (2021) Large circulation patterns strongly modulate long-term variability of Arctic black carbon levels and areas of origin. Geophys Res Lett 48(19) https://doi.org/10.1029/2021GL092876

Stohl A, Berg T, Burkhart JF et al (2007) Arctic smoke – record high air pollution levels in the European Arctic due to agricultural fires in Eastern Europe in spring 2006. Atmos Chem Phys 7:511-534. https://doi.org/10.5194/acp-7-511-2007

Stone RS, Sharma S, Herber A, Eleftheriadis K, Nelson DW (2014) A characterization of Arctic aerosols on the basis of aerosol optical depth and black carbon measurements. Elementa: Science of the Anthropocene 2:000027 https://doi.org/10.12952/journal.elementa.000027

Tomasi, C, Kokhanovsky AA, Lupi A, Ritter C et al (2015) Aerosol remote sensing in polar regions. Earth Sci Rev 140:108-157. https://doi.org/10.1016/j.earscirev.2014.11.001

Winker DM, Vaughan MA, Omar A et al (2009) Overview of the CALIPSO mission and CALIOP data processing algorithms. J Atmos Ocean Tech 26(11):2310-2323. https://doi.org/10.1175/2009JTECHA1281.1

WMO (2016) Aerosol Measurement Procedures, Guidelines and Recommendations, 2nd Edition. WMO No 1177. https://library.wmo.int/doc_num.php?explnum_id=3073

Xian P, Zhang J, O'Neill NT et al (2022a) Arctic spring and summertime aerosol optical depth baseline from long-term observations and model reanalyses – Part 1: Climatology and trend. Atmos Chem Phys 22:9915-9947. https://doi.org/10.5194/acp-22-9915-2022

Xian P, Zhang J, O'Neill NT et al (2022b) Arctic spring and summertime aerosol optical depth baseline from long-term observations and model reanalyses – Part 2: Statistics of extreme AOD events, and implications for the impact of regional biomass burning processes. Atmos Chem Phys 22:9949-9967. https://doi.org/10.5194/acp-22-9949-2022

Zielinski T, Bolzacchini E, Cataldi M et al (2020) Study of Chemical and Optical Properties of Biomass Burning Aerosols during Long-Range Transport Events toward the Arctic in Summer 2017. Atmosphere 11(1):84. https://doi.org/10.3390/atmos11010084

Appendix 1: Ny-Ålesund AOD inter-comparison – details

The PFR is a temperature-stabilised filter radiometer equipped with four interference filters. The calibration of the PFR is performed on a yearly basis at PMOD/WRC against the WMO AOD reference instruments (Kazadzis et al. 2018). The SP1A has been calibrated on an annual or biannual basis using the Langley method during 3-month campaigns at Izaña, Tenerife. Finally, the CIMEL instrument as a part of AERONET is following the standard calibration procedure of the network (Holben et al. 1998).

The basic characteristics of the compared filter radiometers are shown in Table A1.

The comparison has been done against the PFR instruments. Specifically, the PFR AOD measurements at the nominal wavelengths 368, 412, 500 and 862 nm have been compared to the SP1A AOD at the same nominal wavelengths with the actual differences of the centroid wavelengths of the interference filters to be within ±3 nm. For the CIMEL instrument the AOD values at 500 nm, and 870 nm have been directly compared to 500 nm and 862 nm (negligible AOD differences in that spectral region) respectively, while 380 nm and 440 nm (CIMEL) were compared interpolating the PFR-AOD to those wavelengths using the PFR Ångström exponent. The single AOD measurements have been synchronised to ±30 sec time windows.

The differences as a function of time are shown in Figure A1 for PFR and SP1A and in Figure A2 for PFR and CIMEL, while in the right panel the distribution of these differences is given. The normalised distributions are scaled to the percentage of measurements of the peak of the histogram. The overall comparison results are summarised in Table 2 (main document) and the statistics per year in Tables A2 and A3.

The dataset of the PFR instruments is described in 'WORCC-PMOD/WRC quality-assured aerosol optical depth and Ångström exponent for Ny-Ålesund GAW station (2002–present).[1]

Table A1: Basic characteristics of filter radiometers.

	Centroid wavelengths (nm)	Bandwidth (nm)	Field of View (FWHM, deg)	Dataset period	Temperature stabilisation
PFR	368, 412, 500, 862	4-5	2.5	2002-2021	Yes
SP1A	368,412,500,610,675,778,861,945,1020	4-10	2.5	2004-2020	No
CIMEL	340,380,440,500,675,870,945,1020	3-10	1.2	2017-2021	No

1 https://doi.org/10.5281/zenodo.7191072

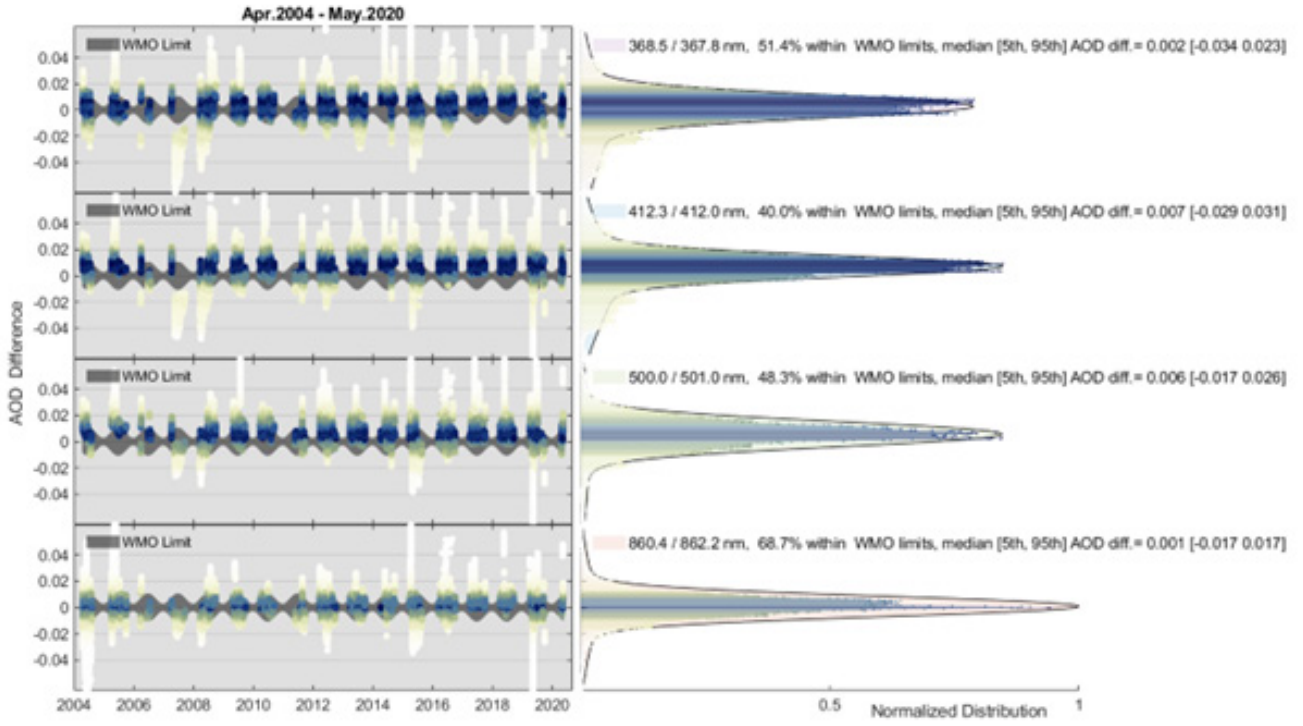

Figure A1: Left panels: AOD difference PFR-SP1A at nominal wavelength 368 nm, 412 nm, 500 nm and 862 nm for the period Apr 2004 to May 2020. The dark shaded area represents the WMO limit for AOD agreement between two instruments. The AOD difference (dots) is coloured based on the probability density function shown in the coloured bars on the right panel. Right panels: Normalised probability density functions of the AOD differences for each wavelength (bars) and approximated by triple gaussian distribution functions (coloured shaded areas).

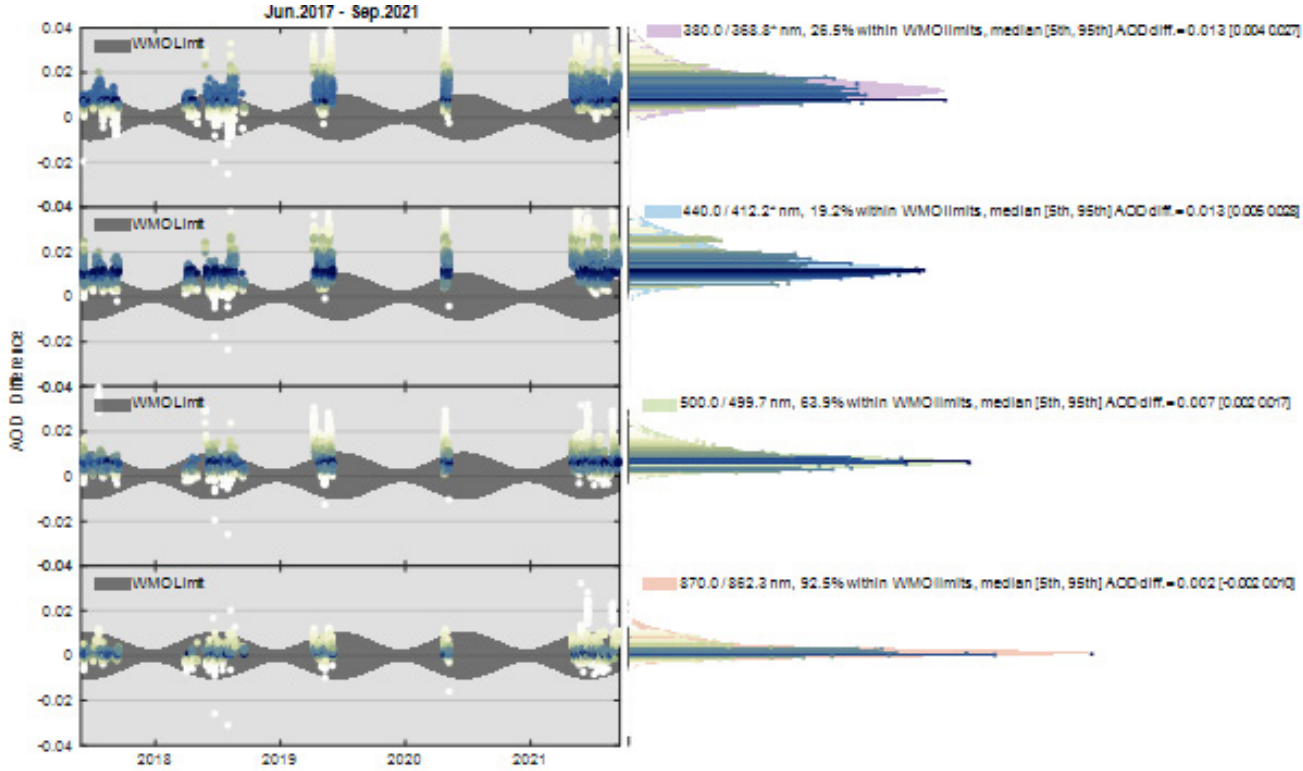

Figure A2: Left panels: AOD difference PFR-CIMEL at nominal wavelength 380 nm, 440 nm, 500 nm and 870 nm for the period Jun 2017 to Sep 2021. The dark shaded area represents the WMO limit for AOD agreement between two instruments. The AOD difference (dots) is coloured based on the probability density function shown in the coloured bars on the right panel. Right panels: Normalised probability density functions of the AOD differences for each wavelength (bars) and approximated by triple gaussian distribution functions (coloured shaded areas).

Table A2: Comparison result of AOD at four common wavelengths between PFR and SP1A. The statistics are presented per year and for the whole dataset.

	Median AOD difference (PFR-SP1A)				Standard deviation				Within WMO limit (%)				Correlation Coefficient				Number of compared points (x1000)
year	368 nm	412 nm	500 nm	862 nm	368 nm	412 nm	500 nm	862 nm	368 nm	412 nm	500 nm	862 nm	368 nm	412 nm	500 nm	862 nm	
2004	-0.007	0.006	0.010	0.006	0.009	0.008	0.009	0.015	54	**67**	44	47	0.982	0.985	0.966	0.487	10
2005	0.005	0.015	0.023	0.017	0.015	0.016	0.012	0.019	54	32	5	21	0.976	0.965	0.967	0.523	4
2006	0.011	0.006	0.016	0.014	0.015	0.013	0.012	0.012	29	32	39	31	0.947	0.952	0.941	0.890	2
2007	-0.031	-0.026	-0.007	-0.009	0.016	0.014	0.009	0.005	1	0	52	40	0.905	0.912	0.935	0.873	17
2008	-0.013	-0.012	0.001	-0.004	0.019	0.021	0.012	0.011	11	10	61	56	0.958	0.941	0.968	0.857	14
2009	0.001	0.000	0.011	0.000	0.008	0.007	0.010	0.005	**85**	**85**	36	**92**	0.984	0.982	0.951	0.909	14
2010	0.004	0.007	0.014	0.003	0.005	0.009	0.005	0.004	**75**	61	14	**93**	0.982	0.932	0.953	0.919	16
2011	-0.003	-0.001	0.003	-0.005	0.009	0.011	0.007	0.007	**85**	**84**	**89**	**74**	0.933	0.878	0.896	0.483	5
2012	0.001	-0.001	0.010	0.002	0.010	0.009	0.009	0.007	**75**	**74**	33	**77**	0.967	0.965	0.944	0.852	24
2013	0.002	0.014	0.008	0.003	0.010	0.010	0.007	0.006	51	13	46	**83**	0.960	0.955	0.953	0.837	23
2014	0.014	0.015	0.011	0.007	0.010	0.008	0.007	0.006	5	2	33	**70**	0.974	0.983	0.974	0.911	15
2015	-0.006	0.001	-0.008	-0.010	0.029	0.028	0.026	0.024	45	60	34	25	0.793	0.756	0.698	0.309	24
2016	0.002	0.006	0.000	-0.001	0.009	0.009	0.007	0.007	**77**	59	**89**	**88**	0.977	0.972	0.971	0.852	32
2017	0.008	0.012	0.009	0.007	0.006	0.009	0.007	0.004	51	15	45	**71**	0.985	0.960	0.953	0.911	20
2018	0.009	0.011	0.007	0.006	0.007	0.007	0.008	0.005	39	15	60	**78**	0.987	0.985	0.965	0.926	18
2019	-0.002	0.004	0.001	-0.002	0.043	0.041	0.038	0.024	46	31	50	55	0.696	0.704	0.598	0.234	19
2020	0.002	0.004	0.003	0.001	0.008	0.007	0.006	0.005	**66**	56	**96**	**98**	0.925	0.905	0.894	0.689	7
All Years	**0.002**	**0.007**	**0.006**	**0.001**	**0.020**	**0.020**	**0.017**	**0.013**	**51**	**40**	**48**	**69**	**0.907**	**0.891**	**0.863**	**0.656**	**265**

Table A3: Comparison result of AOD at four wavelengths between PFR and CIMEL. The PFR-AOD at 380 nm and 440 nm has been retrieved from interpolation of 368 nm and 412 nm AOD using the PFR-AE. The statistics are presented per year and for the whole dataset. Wavelengths marked with * were interpolated using the Ångström exponent to match the CIMEL wavelength.

	Median AOD difference (PFR-SP1A)				Standard deviation				within WMO limit (%)				Correlation Coefficient				Number of compared points
CIMEL	380 nm	440 nm	500 nm	870 nm	380 nm	440 nm	500 nm	870 nm	380 nm	440 nm	500 nm	870 nm	380 nm	440 nm	500 nm	870 nm	
PFR	368 nm*	412 nm*	500 nm	862 nm	368 nm*	412 nm*	500 nm	862 nm	368 nm*	412 nm*	500 nm	862 nm	368nm*	412 nm*	500 nm	862 nm	
2017	**0.006**	**0.007**	**0.005**	**0.001**	**0.003**	**0.003**	**0.002**	**0.001**	**82.4**	**66.4**	**90.8**	**99.5**	**0.97**	**0.98**	**0.96**	**0.97**	666
2018	**0.007**	**0.007**	**0.003**	**-0.001**	**0.004**	**0.004**	**0.003**	**0.003**	**71.1**	**71.2**	**93.2**	**97.7**	**0.99**	**0.99**	**0.98**	**0.96**	789
2019	0.015	0.013	0.008	0.003	0.007	0.006	0.006	0.003	13.7	14.6	52.5	91.4	0.95	0.96	0.92	0.87	747
2020	0.014	0.015	0.010	0.003	0.006	0.006	0.004	0.002	22.9	16.2	39.3	98.0	0.89	0.87	0.91	0.93	1423
2021	0.014	0.015	0.007	0.002	0.005	0.005	0.003	0.003	16.8	7.2	64.3	89.4	0.99	0.98	0.98	0.94	5404
All Years	**0.013**	**0.013**	**0.007**	**0.002**	**0.006**	**0.006**	**0.004**	**0.003**	**26.5**	**19.2**	**63.9**	**92.5**	**0.99**	**0.98**	**0.98**	**0.94**	**8722**